1

Modified Eigen Decomposition based Interval Analysis (MEDIA) for Power System Dynamic State Estimation

Yuting Chen, Student Member, IEEE, Ning Zhou, Senior Member, IEEE, Ziang Zhang, Senior Member, IEEE

Abstract— The Bayesian approach has been used for the dynamic state estimation (DSE) of a power system. However, due to the complexity of noise resources, it is difficult to quantify measurement and process noise using probability density functions (PDFs). To overcome the difficulty, the authors of this paper propose a modified eigen decomposition based interval analysis (MEDIA) method, which employs bounds instead of PDFs to quantify the noise, and uses the eigen decomposition method to reduce the negative impact of the overestimation problem. Using the simulation data generated from IEEE 16-machine and IEEE 10-machine systems, it is shown that the proposed MEDIA method can estimate the hard boundaries of dynamic states in real time. Comparison with the forward-backward propagation method and the extended set-membership filter also shows that the proposed MEDIA method performs better by providing narrower boundaries in the DSE.

Index Terms—Dynamic state estimation, eigen decomposition, interval analysis, power system, state estimation.

I. INTRODUCTION

WITH the widespread deployment of phasor measurement units (PMUs) and advanced communication infrastructure, the Bayesian approach has been proposed to estimate the dynamic states of a power system [1]. In [2]-[5], the extended Kalman filter (EKF) is introduced to estimate the state variables of synchronous generators. However, the EKF suffers a large estimation error or even divergence in a highly nonlinear system. To better deal with nonlinearity, the unscented Kalman filter (UKF) is proposed in [6], and the extended particle filter (PF) is proposed in [7] to estimate the dynamic states. The ensemble Kalman filter (EnKF) is proposed in [8] to estimate the dynamic states and parameters simultaneously. In [9], an EKF method with unknown inputs is introduced to address the scenario where some inputs cannot be directly measured in power systems.

All the above dynamic state estimation (DSE) methods are Bayesian-based filters, which assume that the probability density functions (PDFs) of the measurement and process noise are known at every time instant. However, for a practical power system, this assumption may not always hold. It is suggested in [10] that PMU measurement noise of the voltage and current phasors may not always follow the Gaussian distribution. The noise in measurements may include not only the noise from the instrument inaccuracy but also the noise from external electromagnetic interference, communication channels, and cyberattacks. Due to its complex sources, measurement noise may have significant bias and unknown covariance. The same thing happens with the process noise. When the noise's PDFs are unknown, Bayesian-based filters may have significant estimation errors.

The unknown distributions of measurement and process noises in the DSE motivate the application of interval analysis, which quantifies noise uncertainty through boundaries instead of PDFs. The initial work on interval analysis based DSE(IA-DSE) is presented in [11] and [12], which estimates the ellipsoids that contain the true states when the perturbations and noise are given in boundaries, and later extended to real-life problems in [13]-[15]. However, these algorithms are originally designed for linear systems, which are not suitable for power systems. To overcome this limitation, the interval analysis was further extended for its application to nonlinear systems in [16] and [17]. Another challenge to employing interval analysis in the DSE is the overestimation problem, which often leads to rapidly growing and even divergent boundaries of the estimated states. The overestimation problem and its negative impact are studied and explained through examples in [18]. To mitigate the negative impact of the overestimation problem, the set inversion via interval analysis (SIVIA) method is applied in IA-DSE [19]. However, the low computational efficiency of the SIVIA method makes it unsuitable for real-time applications in power systems. In [20], the IA-DSE is introduced to power system DSE and tested on 2nd and 3rd order systems assuming that some states can be directly measured. It is worth noting that higher-order and more complex systems are more prone to overestimation issues. Such systems tend to suffer from the

This work was supported by the NSF through grant no. #1845523 and by the U.S. Department of Energy's Office of Energy Efficiency and Renewable Energy (EERE) under the Solar Energy Technologies Office Award Number DE-EE0009341. Yuting Chen, Ning Zhou and Ziang. Zhang are with the Department of Electrical and Computer Engineering, Binghamton University, State University of New York, Binghamton, NY, 13902, USA (email: {ychen411, ningzhou, ziang.zhang}@binghamton.edu).

overestimation problem, which can result in extremely large width of the estimated interval.

To address the challenges, a modified eigen decomposition based interval analysis (MEDIA) method is proposed for the DSE in this paper. The proposed MEDIA method can accommodate the boundaries of PMU measurement noise specified by the IEEE standard [21]. In addition, the outputs of the MEDIA method are the upper and lower bounds of the estimated states, which fit many needs of state monitoring and control strategies. The contributions of this paper can be summarized as follows:

- 1) Compared to the conventional forward-backward propagation (FBP) method and the extended set-membership filter (ESMF) method, the proposed MEDIA method can significantly reduce the negative impact of the overestimation problem in the DSE.
- 2) Instead of the estimated PDFs in the Bayesian-based filters, the proposed MEDIA method calculates the hard boundaries of the states, which guarantee to include the true states.
- 3) Compared to the confidence interval built by the Hinfinity unscented Kalman filter (HUKF) method [27], the proposed MEDIA method offers narrower boundaries of the states, which guarantee to include the true states.

The rest of the paper is organized as follows. In Section II, the DSE is formulated into an interval analysis problem and solved using the FBP method. The MEDIA method is proposed to deal with the overestimation problem in Section III. Case studies are carried out in Section IV to evaluate the performance of the MEDIA method. Finally, the conclusions and future work are presented in Section V.

II. PROBLEM FORMULATION

In this section, the basic concepts of interval analysis are reviewed first. Then, the conventional FBP method for interval analysis is described. Finally, the DSE is formulated as an interval analysis problem and solved using the FBP method.

A. Review on Interval Analysis

Interval analysis represents a variable by its upper and lower boundaries, and defines function operations among interval variables. A real-number interval variable [x] is a closed and continuous subset of \mathbb{R} , which can be defined by (1) [22].

$$[x] = [\underline{x}, \overline{x}] = \{x \in \mathbb{R} | \underline{x} \le x \le \overline{x}\}. \tag{1}$$

Here, \underline{x} and \overline{x} are the lower and upper bounds of [x], respectively. For example, if the reading of a voltmeter with 2% accuracy is 100 V, the measured voltage can be denoted as an interval variable of [V]=[98,102] V. Similarly, if the reading of an ammeter with 1% accuracy is 2 A, the measured current can be denoted as an interval variable of [I]=[1.98, 2.02] A.

The intersection and union of two interval variables are defined by (2) and (3), respectively.

$$[x] \cap [y] = \{ z \in \mathbb{R} | z \in [x] \text{ and } z \in [y] \}. \tag{2}$$

 $[x] \cup [y] = |[x] \cup [y]| = [\{z \in \mathbb{R} | z \in [x] \text{ or } z \in [y]\}].$ Here, [] presents the interval hull, which is the smallest interval containing [x]U[y] [16].

Real functions can also be extended to interval functions. Let f be a real function mapping from \mathbb{R}^n to \mathbb{R}^m . Its corresponding interval function [f] is defined by (4) [23], where the [x] is the real interval vector of \mathbb{R}^n , which is an ordered *n*-tuple of intervals.

$$[f]([x]) = [\{f(x_1, ..., x_n) | x \in [x]\}]$$
 (4)

The intersection can be applied to two interval vectors only if they have the same dimension. For example, power [P] can be calculated from the voltage [V] and current [I] by extending conventional operation the of multiplication [P]=[V]*[I]=[98, 102]*[1.98, 2.02]=[194.04, 206.04] W. The intersection interval vector will be empty if any intersection of their corresponding components is empty.

The pseudo volume of an interval vector is defined by (5), where diam $\{\cdot\}$ calculates the diameter of an interval.

$$vol\{[x]\} = \sum_{i=1}^{n_x} diam\{[x_i]\}$$
 (5)

B. Review on the FBP Method

The FBP [24] method is a widely used interval analysis method to solve constraint satisfaction problems (CSPs), which can be defined by (6) [23].

$$\mathcal{H}: (f(x) = 0, x \in [x]). \tag{6}$$

Here,

$$\begin{cases} f_i(\mathbf{x}) = f_i(x_1, ..., x_n) \\ \mathbf{f} = (f_1, ..., f_m)^T \end{cases}$$
The solution set of \mathcal{H} is defined as:

$$S = \{x \in [x] | f(x) = 0\}$$
 (8)

Note that S is not necessarily an interval vector. Utilizing interval analysis, the interval hull of S is the optimal solution, which can be defined by (9).

$$[\mathbf{x}]' = [S] \supseteq S \tag{9}$$

The FBP method contracts \mathcal{H} so that a suboptimal solution [x] can be found via a recursive algorithm, in which $[x] \supseteq$ $[x]' \supseteq S$. The FBP method was chosen as a benchmark method in this paper because it is straightforward to implement and can handle nonlinear models [24].

C. DSE of Power Systems through the FBP

The FBP method can be applied to estimate the upper and lower bounds of the dynamic states of a generator (e.g., rotor angles and speeds) as follows. Assume that a PMU measures the voltage and current phasors at the terminal bus of the target generator. Their measurement noises can be quantified through the upper and lower bounds of interval variables V, θ and I_{mag} , I_{ang} , respectively. Note that because all the variables thereafter will be interval variables, the brackets in their notations are dropped hereafter to be concise. The corresponding real and reactive powers are calculated as $P'_e + jQ'_e =$ $VI_{mag}e^{j(\theta-I_{ang})}$.

The input vector (u), output vector (y) and state vector (x)are defined in (10.a)-(10.c) as interval vectors, and described in Appendix I. Here, P_e 'is the real power calculated from voltage and current phasor measurements. P_e and Q_e are the real power and reactive power calculated from the estimated states through (41)-(47) or (49)-(54).

$$u = [P'_{e} \quad V \quad \theta]^{T}.$$
 (10.a)

$$y = [P_{e} \quad Q_{e}]^{T}.$$
 (10.b)

$$x = [E'_{q} \quad E'_{d} \quad \delta \quad \omega \quad E_{fd} \quad V_{F} \quad V_{R} \quad T_{M} \quad P_{SV}]^{T}.$$
 (10.c)

$$x = [E'_{\alpha} \quad E'_{\beta} \quad \delta \quad \omega) \quad E_{fd} \quad V_F \quad V_B \quad T_M \quad P_{SV}]^T \quad (10 \text{ c})$$

The generator model can be defined as a continuous-time nonlinear state space model (16) in Appendix I. To apply the FBP method, (16) is discretized into the discrete-time model of (10.d) as follows.

$$\begin{cases} x_{k+1} = f(x_k, u_k) + w_k \\ y_{k+1} = g(x_{k+1}, u_{k+1}) + v_{k+1} \end{cases}$$
 (10.d) The FBP can be applied to (10.d) through two stages

iteratively: forward propagation and backward propagation.

- First, assign k=0. Initialize $x_0 = \left[\underline{x_0}, \overline{x_0}\right]$. Here, $\overline{x_0}$ and $\underline{x_0}$ are the upper and lower bounds of the states. Usually, the initial interval x_0 shall be large enough to cover its true values.
- Initialize $x_{k+1} = [x_{lower\ limit}, x_{upper\ limit}].$ (ii)
- In the forward propagation stage, the intervals on the left (iii) side of the constraints (10.d) are contracted through
 - F1: $x_{k+1} = x_{k+1} \cap (f(x_k, u_k) + w_k)$
 - F2: $y_{k+1} = y_{k+1} \cap (g(x_{k+1}, u_{k+1}) + v_{k+1});$ if isempty (y_{k+1}) , go to (vi).
- In the backward propagation stage, all the intervals on the right side of the constraints (10.d) are contracted through.
 - B1: $x_{k+1} = x_{k+1} \cap g^+(y_{k+1}, x_{k+1}, u_{k+1}, v_{k+1})$
 - B2: $x_k = x_k \cap (f^+(x_{k+1}, x_k, u_k, w_k))$
- Repeat (iii) and (iv) until the contractions of x_{k+1} and x_k are smaller than a predetermined threshold.
- (vi) Assign k = k + 1, and go to step (ii).

In step (ii), x_{k+1} can be initialized with the anti-windup limitation and physical limitation. In step (iii), if the resulting y_{k+1} in F2 is empty, the measurement is treated as bad data and

In step (iv), functions g^+ and f^+ in B1 and B2 are the pseudo inverse of functions g and f, respectively. They are constructed to find the x_{k+1} and x_k from y_{k+1} and x_{k+1} . By reducing the dependence problem, the pseudo inverse function can leverage past states. For example, equations (55)-(68) and (70)-(83) in Appendix II show the standard pseudo inverse of function g, and equations (69) and (84) are further developed to reduce the overestimation caused by the dependence problem during the backward propagation.

Following the procedure steps (i)-(vi) above, the FBP method can calculate the upper and lower bounds of the dynamic states of a generator. Yet, as it will be shown in the case studies in Section IV, the bounds of the states may grow rapidly with time and quickly out of reasonable ranges, which makes the estimation results not useful in guiding operations.

III. CHALLENGES OF OVERESTIMATION AND THE PROPOSED **SOLUTIONS**

The FBP method is a rigorous interval analysis process, which implies all the possible values of the arguments are guaranteed to be enclosed in the resulting intervals. However, the resulting intervals may also include spots that are not part of the actual solution set, which is known as the overestimation

problem [22]. In regular interval computing, overestimation is usually neglectable. But it presents a significant challenge to the DSE because, in the forward propagation step of each time instant, the state transition function rotates and scales the state intervals, which leads to growing intervals along the direction of each individual state. Without proper control, the resulting state intervals may keep growing with time to include more and more unnecessary spots, which can eventually compromise the application value of estimated intervals. To reduce the overestimation, the authors propose an eigen decomposition based approach in subsection B for a linear system, and then modify it for the nonlinear system of a generator model in subsection C.

A. Overestimation Problem

Both the dependence problem and the wrapping effect contribute to the overestimation problem in the DSE. Readers are referred to [22] for their detailed descriptions and examples. A brief overview is provided as follows for this paper to be selfcontained.

Dependence problem

When an interval variable appears multiple times in the expression to be evaluated, the dependence problem develops because each appearance is treated as an independent variable during interval calculation. As such, to reduce the dependence problem, the authors of this paper have tried to simplify the formulas to be evaluated symbolically by factoring out common terms. For example, in addition to inputs, outputs, and states, equations (55)-(68) and (70)-(83) have involved serval intermedia variables, such as V_d , V_q , I_d and I_q . They all depend on the inputs, outputs and states, and appear in the equations multiple times, which will lead to the dependence problem. To reduce the overestimation from the dependence problem, equations (69) and (84) are created without these redundant variables.

2) Wrapping effect

The wrapping effect can also cause overestimation in interval contractor. Because only axis-parallel boxes are used for interval computing, axis-parallel boxes are wrapped around non-axis-parallel areas in the solution space, which comprise not only the precise solution but also physically impossible points. As such, to reduce the negative impact of the wrapping effect, one should try to reduce rotating operations when possible.

B. Eigen decomposition based Interval Analysis (EDIA) Method

To suppress the overestimation of the FBP from the wrapping effect and dependence problem during the DSE of a linear system, the authors propose an EDIA method as follows. Assume that a system can be described by the linear state space model (11).

$$\begin{cases} x_{k+1} = Ax_k + Bu_k + w_k \\ y_{k+1} = Cx_{k+1} + Du_{k+1} + v_{k+1} \end{cases}$$
 (11)

Here, x_k , u_k , y_k are the states, inputs, and measurements at time k, respectively. $A \in R^{n_x \times n_x}$, $B \in R^{n_x \times n_u}$, $C \in R^{n_y \times n_x}$ and $D \in \mathbb{R}^{n_y \times n_u}$ are the constant matrices. w_k and v_{k+1} are the noises of the state transition function and the measurement function, respectively, which include time discretization and model approximation errors, etc.

To reduce the wrapping effect, an auxiliary vector x'_k is introduced through (12).

$$x'_k = Q^{-1}x_k \tag{12}$$

Here, $Q \in R^{n_\chi \times n_\chi}$ and i^{th} column of Q is the right eigenvector q_i of matrix A. Then, the original system (11) can be transformed into (13) by replacing x_k with x'_k .

$$\begin{cases} x'_{k+1} = Q^{-1}AQx'_{k} + Q^{-1}Bu_{k} + Q^{-1}w_{k} & (13. a) \\ = \Lambda x'_{k} + Q^{-1}Bu_{k} + Q^{-1}w_{k} & (13. b) \end{cases}$$
Here, Λ is a diagonal matrix whose diagonal elements are the

corresponding eigenvalues of matrix A, $\Lambda_{ii} = \lambda_i$. Note that in (13.a), every element in the state x'_k is updated independently, i.e., $x_{k+1}^{\prime i} = \lambda_i x_k^{\prime i}$ in the prediction step. As such, the overestimation problem associated with the dependence problem and the wrapping effect can be significantly reduced in the transformed dynamic system (13).

C. Modified EDIA (MEDIA) Algorithm

The proposed EDIA is modified to estimate states of generators, which has a nonlinear model. The MEDIA method is proposed here to combine the advantage of lower overestimation in the EDIA and applicability to a nonlinear system in the FBP. Consider the discrete-time equations for a nonlinear dynamical system in (14).

$$\begin{cases} x_{k+1} = h(x_k, u_k) + w_k \\ y_{k+1} = g(x_{k+1}, u_{k+1}) + v_{k+1} \end{cases}$$
 Here, h is the state transition function from $R^{n_x} \times R^{n_u}$ to R^{n_x} ,

and g is the measurement function from $R^{n_x} \times R^{n_u}$ to R^{n_y} . To apply the proposed EDIA, (14) is modified to separate its linear and nonlinear terms as (15).

$$x_{k+1} = Ax_k + Bu_k + \Delta h(x_k, u_k) + w_k$$

= $Ax_k + Bu_k + w'_k(x_k, u_k)$, (15.a)

where

$$w'_{k}(x_{k}, u_{k}) = \Delta h(x_{k}, u_{k}) + w_{k}.$$
 (15.b)

Here, A, B represent the linear components of the function h, while Δh is the nonlinear component of the function h. For example, I_d in equation (18) and I_q in equation (19) shall be considered as nonlinear component and included in Δh .

Merging the nonlinear components into the process and measurement noise through the equation (15.b), the MEDIA can be applied to estimate the states of the modified model.

In summary, the MEDIA method can be implemented as follows:

MEDIA:

Initialize x_0 with physical limit and engineering knowledge. $x_0' \leftarrow Q^{-1}x_0$ for k = 1 to k_{end} Initialize $x_{k+1} \leftarrow [x_{lower\ limit}, x_{upper\ limit}]$ $x'_{k+1} \leftarrow [-inf, inf]$ MEDIA updates: $1.\; x_{k+1}^{'} \leftarrow x_{k+1}^{'} \cap \left(\Lambda x^{'}_{\;\;k} + Q^{-1}Bu_{k} + Q^{-1}w^{'}_{\;\;k}(x_{k},u_{k}) \right)$ 2. $x_{k+1} \leftarrow x_{k+1} \cap (Qx_{k+1})$ Apply FBP:

```
3. x_{k+1} \leftarrow x_{k+1} \cap (h(x_k, u_k) + w_k)
      4. y_{k+1} \leftarrow y_{k+1} \cap (g(x_{k+1}, u_{k+1}) + v_{k+1})
      5. If isempty (y_{k+1}), continue
      6. x_{k+1} \leftarrow x_{k+1} \cap g^+(y_{k+1}, x_{k+1}, u_{k+1}, v_{k+1})
      7. x_k = x_k \cap (h^+(x_{k+1}, x_k, u_k, w_k))
      8. x'_{k+1} = x'_{k+1} \cap (Q^{-1}x_{k+1})
end for
```

Here, the states are predicted in steps 1-5 using (15). Step 5 is to detect bad data and mitigate its negative impacts. The predicted states are then corrected in steps 6-8 to update their intervals based on the measurements using (55)-(102) in Appendix II. Note that the intersections of the estimated intervals from the proposed MEDIA method and the FBP method are used as the new estimate. The procedure guarantees that the new method can achieve estimation intervals that are narrower than or equal to each individual method with guaranteed hard boundaries.

IV. CASE STUDIES

In this section, the performance of the proposed MEDIA method is evaluated and compared with the FBP [24], extended set-membership filter (ESMF) [20], and HUKF [27] methods using simulation data from the 10-machine 39-bus system as well as the 16-machine 68-bus system. In addition, the implementation efficiency of the MEDIA method is improved to ensure that it can perform the DSE in real time.

A. Simulations using the 10-Machine 39-Bus System

To evaluate the efficacy and robustness of the interval analysis results, time-domain simulations are carried out using the IEEE 10-machine 39-bus system (shown in Fig. 1) to generate all the true values of the dynamic states and measurement variables. The parameters of the system are taken from [25]. Its synchronous generators with governor and exciter control systems are modeled by equations (18)-(26) in Appendix I through a 9th order differential equation and simulated using the 2nd order Runge-Kutta method. To estimate the dynamic states of generator G5, assume that a PMU is set up at its terminal bus (i.e., bus 34) to measure its voltage phasor $(V \angle \theta)$, current phasor $(I_{mag} \angle I_{ang})$ at 60 samples/s. Bounded intervals of [-0.001, 0.001] are used to mimic the measurement noises added to their true values as follows:

- $I_{mag}^{measured} \sim I_{mag}^{true} + [-0.001, 0.001]$ in per-unit (pu),

- $\theta^{mearsued} \sim \theta^{true} + [-0.001, 0.001]$ in radian.

The real and reactive powers are calculated through the interval multiplication of the simulated voltage and current phasors.

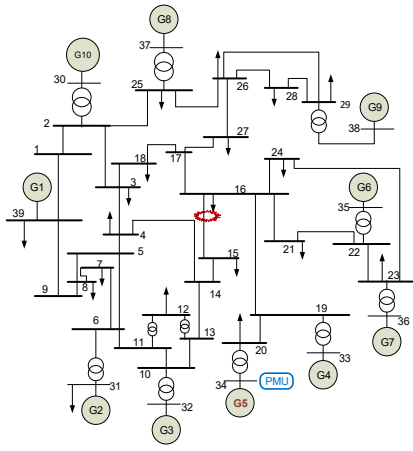


Fig. 1. One-line diagram of the IEEE 10-machine 39-bus system [25].

1) Case I: Steady State Test

In this case study, the proposed MEDIA method is compared with the FBP method [24] and the ESMF method [20] in its capabilities of handling the overestimation problem in the DSE during steady-state responses. To mimic the system's steady-state responses, no major outside disturbance is injected into the system so that all the dynamic states remain constant during the simulation of 50 s. For better illustration, all the algorithms are initialized with the ideal initial condition, $x_0 = x_0^{true} + [-1 \times 10^{-5}, 1 \times 10^{-5}]$, and the DSE is performed during the steady state responses of the system. The measurement noises are simulated using white noises, which are uniformly distributed between -0.001 and 0.001. Due to the space limitation, only the states of generator G5 are estimated with its terminal voltage phasor and real power as model input.

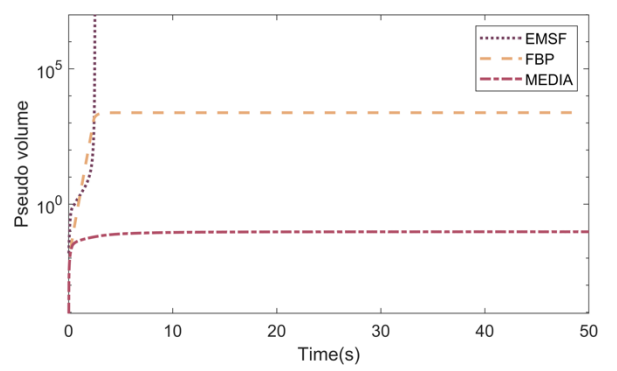
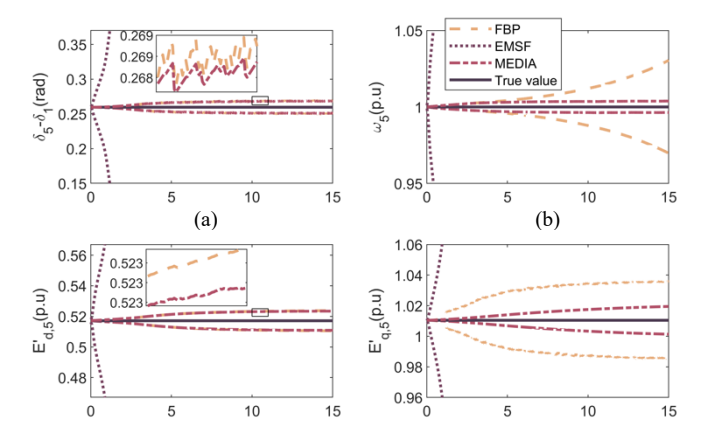


Fig. 2. Pseudo volume of the estimated states using the proposed MEDIA method, the FBP method and the ESMF during the steady-state responses.



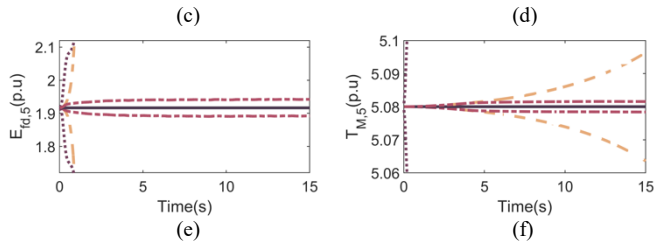
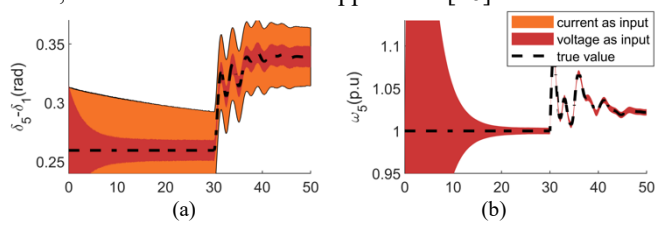


Fig. 3. Estimated states using the proposed MEDIA method, the FBP method and the ESMF during the steady-state responses.

The estimation results are summarized in Fig. 2 and Fig. 3. Note that the pseudo volume defined in (5) is used as a metric in Fig. 2 to evaluate the performance of a DSE method. A smaller pseudo volume indicates less overestimation problem. In Fig. 2, the pseudo volumes of the proposed MEDIA method are smaller than those of the FBP and EMSF methods, which suggests that the MEDIA method has significantly reduced the overestimation problems in its estimated intervals. Also, it can be observed in Fig. 3 that the true states stay inside the estimated intervals of all the three methods. In addition, the proposed MEDIA method has the smallest interval width. In comparison, the EMSF method has the largest interval width, and the volume from the FBP method is in the middle. More specifically, the interval widths of all the states estimated by the EMSF method grow exponentially in the DSE, which disqualifies the EMSF method in the power system DSE. In addition, the interval widths of ω , T_M and E_{fd} estimated by the proposed MEDIA method are significantly smaller than those from the FBP method, which suggests that the proposed MEDIA method can more effectively reduce the negative impact of the overestimation problem than the FBP method in the DSE.

2) Case II: Transient Response Test

In this case study, the proposed MEDIA method is applied to estimate the intervals of the dynamic states during the transient responses using two estimation models. As it is shown in Fig. 1, to incur transient responses, a large disturbance is introduced to the system at t = 30 s by opening the transmission line between buses 15 and 16. The initial state intervals are set with 5 percent of their normal value from their true state as boundaries, $x_0 = x_0^{true} + [-0.05,0.05] * x_0^{true}$. The bounded measurement noises are simulated using white noises, which are uniformly distributed between -0.001 and 0.001. The proposed MEDIA method is implemented for the voltage-input estimation model and current-input estimation model, which are described in Appendix I [26].



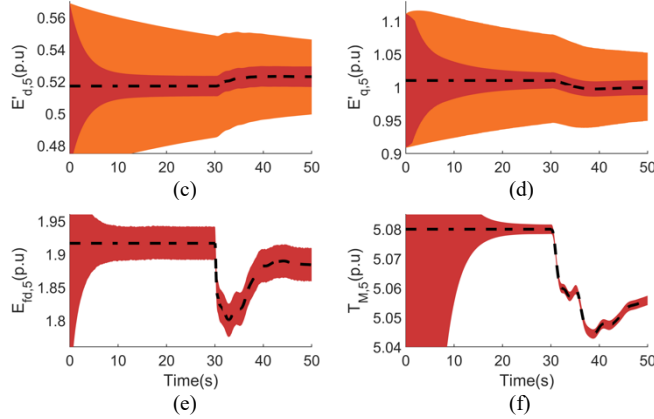
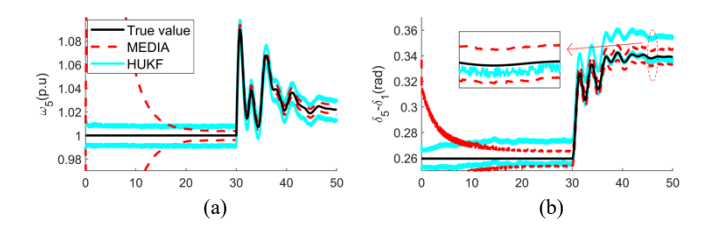


Fig. 4. States estimated by the proposed MEDIA method using the voltageinput estimation model and the current-input estimation model during the transient responses.

The estimation results are summarized in Fig. 4. The estimated states are plotted as the orange and red areas that are defined by upper and lower bounds. The true state values from the simulation are shown in dot lines. It can be observed that the states estimated by the proposed MEDIA method quickly converge to stable interval widths within 30 seconds. The interval widths of the estimated δ , E_d' and E_q' are smaller with the voltage-input estimation model than the current-input estimation model. The MEDIA method has the capability to track all the states and gives the boundaries that always include the true states. Similar results are obtained for case studies with biased initial conditions and not detailed here to stay concise.

3) Case III: Comparison with the HUKF

In this study, the confidence intervals generated by the HUKF [27] and MEDIA methods are compared in the presence of bounded measurement noise. Assume that the measurement noise follows a bimodal distribution that is uniformly distributed around the upper and lower bounds, i.e., $[-1 \times$ 10^{-3} , -0.9×10^{-3}] \cup [0.9×10^{-3} , 1×10^{-3}]. Assume that the DSE method only has access to the measurement's upper and lower boundaries instead of its PDF. To apply the HUKF method, the measurement standard deviation is set to one-sixth of the interval width of the measurement noise. The upper/lower boundaries of the estimation intervals are constructed by adding/subtracting three standard deviations to/from the estimated states. The boundaries and confidence intervals generated by the MEDIA and HUKF methods are summarized in Fig. 5. Here, the red dotted line represents the MEDIA boundaries, and the blue line represents the HUKF confidence intervals. The black line indicates the true value.



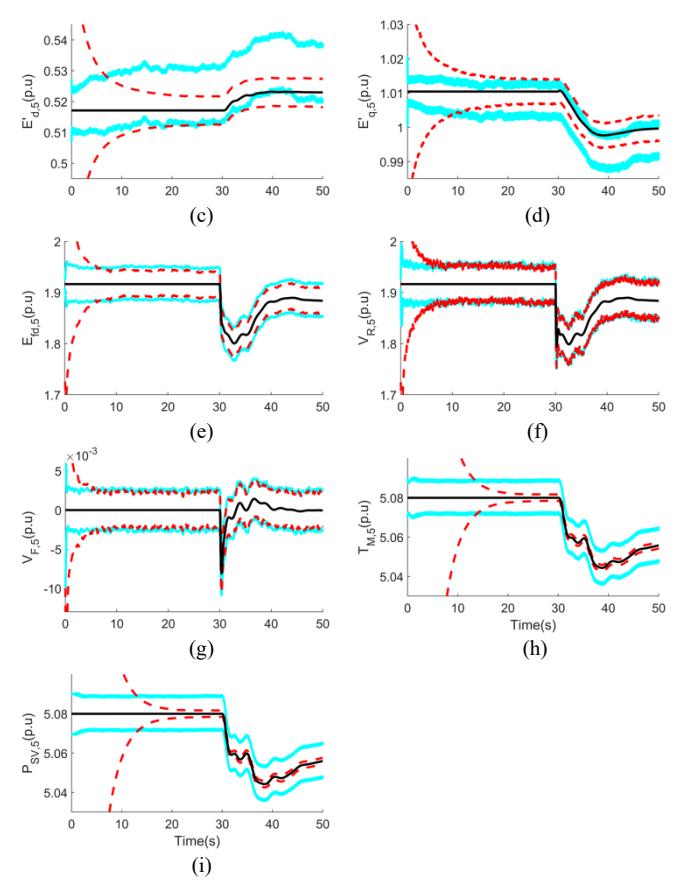


Fig. 5. Estimated states using the proposed MEDIA method and the HUKF method under bimodal distribution noise.

It can be observed that the true states of δ , E'_d , and E'_q fall out of the confidence intervals estimated by the HUKF method. Meanwhile, the HUKF and MEDIA methods produce similar intervals that cover the true value in E_{fd} , V_R , and V_f . In addition, the MEDIA method generates narrower intervals than the HUKF method in ω , T_M , and P_{SV} . It is worth noting that the true states always fall into the intervals estimated by the MEDIA method. The study shows that the proposed MEDIA method is more robust than the HUKF method in that its estimated intervals always include true states.

B. Simulations using the 16-Machine 68-Bus System

To verify the performance of the proposed MEDIA method in a more complex system using a higher-order model, timedomain simulations are carried out using the IEEE 16-machine 68-bus system (shown in Fig. 6) to generate all the true values of the dynamic states and measurement variables. The parameters of the system are taken from [29]. Its synchronous generator is simulated by a sub-transient model [30] with an IEEE Type DC1 excitation system [31] and a turbine-governor system which are modeled by equations (27)-(39) in Appendix I through 11th-order differential equations. There are more nonlinear variables in this model, like the saturation function in equation (39), which challenges the MEDIA method. The simulation is carried out using the Power System Toolbox (PST) [28]. To incur dynamic responses, a three-phase fault is set off at t=30.10 s on the branch between buses 5 and 8. The fault is clear at t=30.15 s at its near end of bus 5, and at t=30.20

s at its far end of bus 8 by tripping off the faulty branch. A PMU is set up on the terminal bus of generator G1 and collects phasor measurements at 100 samples/s. The measurements' noise follows the same distribution as the previous case. To reduce the negative impact of the non-linearity on the DSE, linear interpolation is employed here to increase the effective sampling rate to 200 samples/s [32].

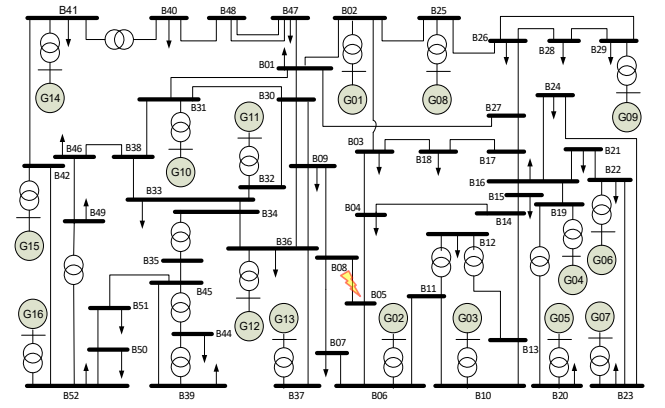
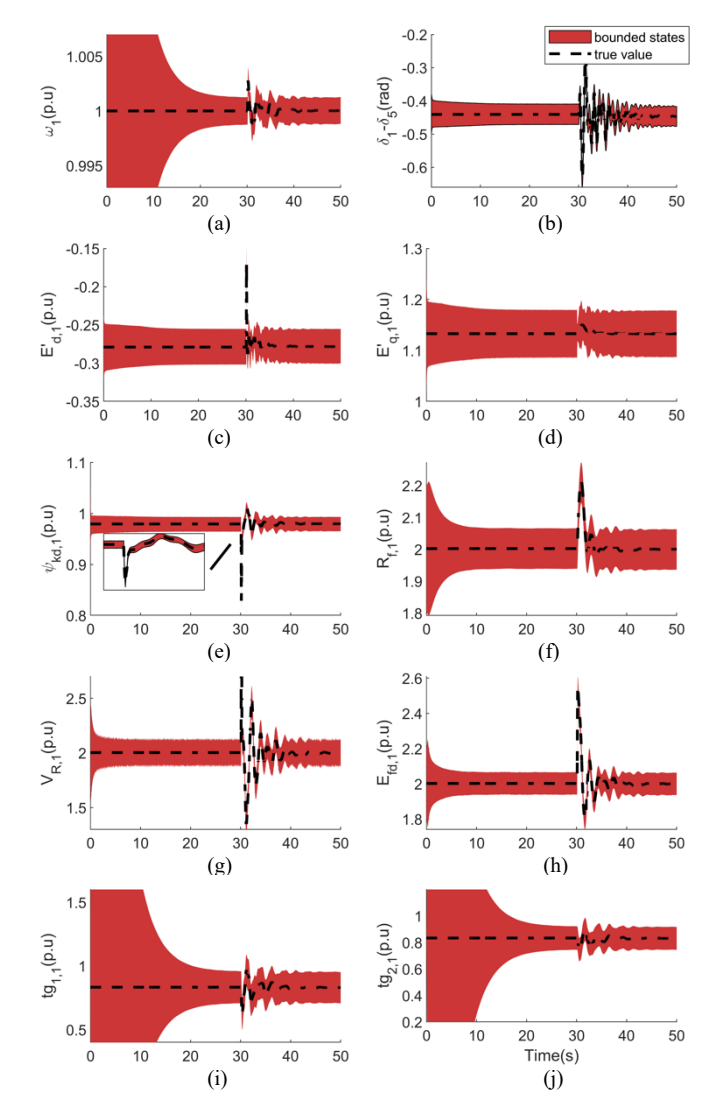


Fig. 6. One-line diagram of the IEEE 16-machine 68-bus system with the faulty line marked out [33].



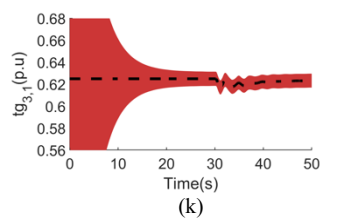


Fig. 7. Estimated states using the voltage-input estimation model and the proposed MEDIA method during the transient responses.

The estimation results are summarized in Fig. 7. It can be observed that the proposed MEDIA method gives the boundaries with reasonable interval width for all the estimated states. Taking advantage of the high sample rate, most of the states converge quickly from the initial intervals. States ω , tg_1 , tg_2 and tg_3 take a longer time duration to converge. It can be observed in the figure that the initial intervals of these states are way wider than the setting initial intervals. This was due to the overestimation during the conversion from X_0 to X_0' . It takes about 30 seconds for these states to converge to stable interval widths.

C. Computational Efficiency

To test the computational efficiency of the proposed MEDIA method, MATLAB was used to implement the algorithm and tested on a PC with an Intel Core i7, 3.20 GHz processor, and 16 GB of RAM. The computation time for assimilating the measurements of one time instant was recorded to evaluate whether the algorithm can run in real time. The statistics on the computation time were obtained from 3,000 sampling instances and presented as ($mean \pm standard\ deviation$) for two different implementations, as follows:

- 63.88 ± 0.05 ms (implementation using INTLAB),
- 2.59 ± 0.01 ms (bound-focused code implemented by the authors).

Initially, the proposed MEDIA method was implemented using INTLAB [34], a toolbox designed for accurately implementing interval analysis algorithms by overloading MATLAB operators. However, the implementation using INTLAB was found to have low computational efficiency. Considering the sampling interval of a PMU with a reporting rate of 100 samples/s is 10 ms, the implementation using INTLAB cannot keep up with the stream of the measurement data in real time. To improve the computation efficiency, the authors modified the initial INTLAB implementation code by removing the calculation for rounding errors and focusing only on bound calculation. Because the rounding errors are negligibly small compared to the measurement and process noises in the proposed application, the modified code can achieve virtually the same accuracy as the original INTLAB code. At the same time, it reduces the calculation time from 63.88 ms to 2.59 ms, which makes it possible to run in real time.

V. CONCLUSIONS AND FUTURE WORK

In this paper, the MEDIA method is proposed to perform the DSE of synchronous machines in power systems under the framework of interval analysis. Different from the Bayesian approach, the proposed MEDIA method uses interval bounds

(instead of PDFs) to quantify noise uncertainty, and offers guaranteed hard boundaries for each estimated state. Leveraging the eigen decomposition, the proposed method can reduce the negative impacts from the wrapping effects and dependence problem of overestimation. Compared with the FBP method and the ESMF method, the proposed MEDIA method can reduce the overestimation in the high-order control system of synchronous machines and give narrower intervals. Compared with the confidence intervals bulit by the HUKF, MEDIA method offer narrower interval and promise to cover the true value. The case studies show the feasibility of the proposed MEDIA algorithm for handling the different generator models and offering guaranteed state boundaries in estimating dynamic states in real time.

In this paper, the interval width of the process noise has been set as a constant interval to stay concise. Follow-up studies will be carried out to adaptively adjust it based on the estimated process noise to improve estimation accuracy. In addition, future work will include studies on how the IA-DSE method can work with a point estimation method and provide valuable complementary information.

APPENDIX I. STATE TRANSITION AND MEASUREMENT MODELS OF SYNCHRONOUS MACHINES

In general, the dynamic behaviors of a synchronous machine can be described by the differential algebraic equation of (16), which includes a state transition function h(*) and a measurement function g(*). These functions are detailed in the following subsections.

$$\begin{cases} \frac{dx}{dt} = h(x, u) + w & (16.a) \\ y = g(x, u) + v & (16.b) \end{cases}$$

A. State Transition Function

The state transition function h(*) of a synchronous machine can be described using differential equations. The 9th-order model and 11th-order model that are used in the paper are described as follows.

1) Model I: the 9th-Order Model

Define the state vector as

$$x = \begin{bmatrix} E'_q & E'_d & \delta & \omega & E_{fd} & V_F & V_R & T_M & P_{SV} \end{bmatrix}^T.$$
 (17)

The following 9th-order differential equation can be used to model the dynamics of governors, exciters, and synchronous generators.

• Synchronous generator:

$$T'_{d0}\frac{dE'_q}{dt} = -E'_q - (X_d - X'_d)I_d + E_{fd}$$
 (18)

$$T'_{q0} \frac{dE'_d}{dt} = -E'_d - (X_q - X'_q)I_q$$
 (19)

$$\frac{d\delta}{dt} = \omega - \omega_s \tag{20}$$

$$\frac{2H}{\omega_s}\frac{d\omega}{dt} = T_M - P'_e - D(\omega - \omega_s)$$
 (21)

• Exciter:

$$T_E \frac{dE_{fd}}{dt} = -K_E E_{fd} + V_R \tag{22}$$

$$T_F \frac{dV_F}{dt} = -V_F + \frac{K_F}{T_E} \left(V_R - K_E E_{fd} \right) \tag{23}$$

$$T_A \frac{dV_R}{dt} = -V_R + K_A \left(V_{ref} - V_F - V \right) \tag{24}$$

· Governor:

$$T_{CH}\frac{dT_M}{dt} = -T_M + P_{SV} \tag{25}$$

$$T_{SV}\frac{dP_{SV}}{dt} = -P_{SV} + P_C - \frac{1}{R_D} \left(\frac{\omega}{\omega_s} - 1\right)$$
 (26)

Here, ω and δ represent the rotor speed and rotor angle, respectively. E'_q and E'_d represent the q-axis and d-axis transient voltage, respectively. E_{fd} , V_F , V_R represent the field voltage, the scaled output of the stabilizing transformer, and the scaled output of the amplifier, respectively. T_M and P_{SV} represent the synchronous machine mechanical torque and steam valve position, respectively. T'_{d0} , T'_{d0} , T_E , T_F , T_A , and T_{SV} represent the corresponding time constants, in seconds. K_E , , and K_A represent the controller gains. V_{ref} and P_c represent the known control inputs. X_d , X'_d , X_q , X'_q represent the d-axis synchronous reactance, transient reactance, q-axis synchronous reactance and transient reactance, respectively. Note that P'_{ρ} represents the real electrical power as an input. I_d and I_q represent the d-axis and q-axis currents, respectively. They are the variables which need to be constructed from input u and state x.

2) Model II: the 11th-Order Model

Define the state vector as

$$\begin{aligned}
 x &= [\delta \quad \omega \quad E'_q \quad E'_d \quad \psi_{kd} \\
 E_{fd} \quad V_R \quad R_f \quad tg_1 \quad tg_2 \quad tg_3].
 \end{aligned}
 \tag{27}$$

The following 11th-order differential equation can be used to model the dynamics of governors, exciters, and synchronous generators.

• Synchronous generator:

$$T'_{d0} \frac{dE'_q}{dt} = (E_{fd} - sat_1 E'_q{}^2 - sat_2 E'_q - sat_3 - \frac{(x_d - x'_d)(x'_d - x''_d)}{(x'_d - x_l)^2} (E'_q - \psi_{kd})$$

$$- \frac{(x_d - x'_d)(x''_d - x_l)}{x'_d - x_l} I_d)$$
(28)

$$T'_{q0} \frac{dE'_d}{dt} = \left(-E'_d - \frac{\left(x_q - x'_q \right) \left(x''_q - x_l \right)}{x'_q - x_l} I_q \right) \tag{29}$$

$$T_{d0}^{"}\frac{d\psi_{kd}}{dt} = (-\psi_{kd} + E_q' - (x_d' - x_l)I_d)$$
 (30)

$$\frac{d\delta}{dt} = 2\pi\omega_0(\omega - 1) \tag{31}$$

$$\frac{d\omega}{dt} = \frac{1}{2H} \left(tg_3 + \frac{T_4}{T_5} \left(tg_2 + \frac{T_3}{T_C} tg_1 \right) - P'_e \right)$$
 (32)

Evciter

$$T_{A} \frac{dV_{R}}{dt} = (-V_{R} + K_{A} * V_{A})$$
 (33)

$$T_E \frac{dE_{fd}}{dt} = (V_R - K_E E_{fd} - SE)$$
 (34)

$$T_F \frac{dR_f}{dt} = (-R_f + E_{fd}) \tag{35}$$

Governor:

$$T_S \frac{dtg_1}{dt} = (P_{m0} + (1 - \omega)/R - tg_1)$$
 (36)

$$T_C \frac{dtg_2}{dt} = \left(\left(1 - \frac{T_3}{T_C} \right) tg_1 - tg_2 \right) \tag{37}$$

$$T_{5} \frac{dtg_{3}}{dt} = \left(\left(1 - \frac{T_{4}}{T_{5}} \right) \left(tg_{2} + \frac{T_{3}}{T_{C}} tg_{1} \right) - tg_{3} \right)$$
 (38)

in which

$$S_{E} = \begin{cases} Ae^{B|E_{fd}|} & for E_{fd} > 0\\ -Ae^{B|E_{fd}|} & for E_{fd} < 0. \end{cases}$$
(39)

Here, ψ_{kd} represents the flux on d-axis. x_d , x_d' and x_d'' represent synchronous reactance, transient reactance, and subtransient reactance on d-axis, respectively. x_q , x'_q and x''_q represent synchronous reactance, transient reactance, and subtransient reactance on q-axis, respectively. x_l represents the leakage reactance. sat_1 , sat_2 and sat_3 represent the field saturation factors. R_f and S_E represent the stabilizing transformer state variable and saturation function in the exciter, respectively. tg_1 , tg_2 and tg_3 represent the governor state variable, servo state variable and reheater state variable, respectively. T_S , T_C , T_3 , T_4 and T_3 represent their corresponding time constants.

B. Measurement Function

The measurement function g(*) of a synchronous machine can be described using algebraic equations. There are many approaches of setting measurements for the DSE. The two estimation models, i.e., the voltage-input estimation model and current-input estimation model, are used in this paper and detailed as follows.

Estimation model that uses voltage phasors as inputs

Define the input vector as

$$u_V = [P'_e \quad V \quad \theta \quad V_{ref} \quad P_C]^T \tag{40}$$

Here, V and θ represent the terminal bus voltage magnitude and phase angle, respectively. V_{ref} and P_c represent the controller inputs, which are modeled by interval variables whose bounds are set up according to the accuracy of measurements. To form the state transition function $h_n(*)$, I_d and I_q in (18)-(19) and (28)-(30) can be calculated in term of input u_v and states x as in (41)-(44).

$$V_d = V\sin\left(\delta - \theta\right) \tag{41}$$

$$V_a = V\cos\left(\delta - \theta\right) \tag{42}$$

$$V_{q} = V\cos(\delta - \theta)$$

$$I_{d} = \frac{E'_{q} - V_{q}}{X'_{d}}$$

$$(43)$$

$$I_{q} = -\frac{E_{d}^{\prime} - V_{d}}{X_{d}^{\prime}} \tag{44}$$

Define the output vector as

$$y = [P_e \quad Q_e]^T \tag{45}$$

Here P_e and Q_e represent the real and reactive electrical power outputs of the generator. To form the measurement function $g_V(*)$, P_e and Q_e can be calculated from input u_V and states x as in (46)-(47).

$$P_e = V_d I_d + V_a I_a \tag{46}$$

$$\begin{aligned} P_e &= V_d I_d + V_q I_q \\ Q_e &= V_q I_d - V_d I_q \end{aligned} \tag{46}$$

2) Estimation model that uses current phasors as inputs Define the input vector as

$$u_I = [P'_e \quad I_{mag} \quad I_{ang} \quad V_{ref} \quad P_C]^T, \tag{48}$$

 $u_I = [P'_e \quad I_{mag} \quad I_{ang} \quad V_{ref} \quad P_C]^T, \tag{48}$ where I_{mag} and I_{ang} are the current magnitude and current angle at the global reference.

To form the state transition function $h_I(*)$, I_d and I_q in (18)-(19) and (28)-(30) can be calculated from input u_I and states x

$$I_d = I_{mag} \sin \left(\delta - I_{gng}\right) \tag{49}$$

$$I_d = I_{mag} \sin \left(\delta - I_{ang}\right)$$

$$I_q = I_{mag} \cos \left(\delta - I_{ang}\right)$$
(50)

This model uses the same output vector as in (45). To form the measurement function $g_I(*)$, P_e and Q_e can be calculated from input u_I and states x as in (51)-(54).

$$V_d = E_d' + I_a X_a' \tag{51}$$

$$V_q = E_q' - I_d X_d' \tag{52}$$

$$V_{d} = E'_{d} + I_{q}X'_{q}$$
 (51)

$$V_{q} = E'_{q} - I_{d}X'_{d}$$
 (52)

$$P_{e} = V_{d}I_{d} + V_{q}I_{q}$$
 (53)

$$Q_{e} = V_{q}I_{d} - V_{d}I_{q}$$
 (54)

$$Q_e = V_a I_d - V_d I_a \tag{54}$$

APPENDIX II. BACKWARD PROPAGATION MODELS FOR THE FBP METHOD

Because the forward propagation model in the FBP method is straightforward, only the backward propagation model is given in this appendix.

For the output function $g_V(*)$, the backward propagation model can be summarized as in (55)-(68).

$$V_{q} = V_{q} \cap [(P_{e} - V_{d}I_{d})/I_{q}]$$

$$I_{q} = I_{q} \cap [(P_{e} - V_{d}I_{d})/V_{q}]$$
(55)
(56)

$$I_q = I_q \cap [(P_e - V_d I_d)/V_q] \tag{56}$$

$$V_d = V_d \cap [(P_e - V_d I_d)/I_d]$$
 (57)

$$I_d = I_d \cap [(P_e - V_d I_d)/V_d]$$

$$V_q = V_q \cap [(Q_e + V_d I_q)/I_d]$$
(58)
(59)

$$V_a = V_a \cap \left[(Q_e + V_d I_a) / I_d \right] \tag{59}$$

$$I_d = I_d \cap [(Q_e + V_d I_q)/V_q] \tag{60}$$

$$V_d = V_d \cap [(V_q I_d - Q_e)/I_q]$$
 (61)

$$I_{q} = I_{q} \cap [(V_{q}I_{d} - Q_{e})/V_{d}]$$

$$V_{d} = V_{d} \cap [E'_{d} + I_{q}X'_{q}]$$
(62)
(63)

$$V_d = V_d \cap [E'_d + I_a X'_a] \tag{63}$$

$$E'_{d} = E'_{d} \cap [V_{d} - I_{a}X'_{a}] \tag{64}$$

$$V_a = V_a \cap [E_a' - I_d X_d'] \tag{65}$$

$$F' = F' \cap [V + I, X'] \tag{66}$$

$$E'_{d} = E'_{d} \cap [V_{d} - I_{q}X'_{q}]$$

$$V_{q} = V_{q} \cap [E'_{q} - I_{d}X'_{d}]$$

$$E'_{q} = E'_{q} \cap [V_{q} + I_{d}X'_{d}]$$

$$(66)$$

$$E'_{q} = E'_{q} \cap [V_{q} + I_{d}X'_{d}]$$

$$(66)$$

$$\delta = \delta \cap \left[a \sin \left(\frac{v_d}{v} \right) + \theta \right] \tag{67}$$

$$\delta = \delta \cap \left[a\cos\left(\frac{V_q}{V}\right) + \theta \right] \tag{68}$$

To further suppress the overestimation in the measurement equations, a simplified equation for δ is employed as (69).

$$\delta = \operatorname{atan}\left(\frac{E'_d}{E'_q}\right) + \operatorname{atan}\left(\frac{P_e}{Q_e + V_{mag}^2/X_d'}\right) + V_{ang}$$
 (69)

For the output function $g_I(*)$, the backward propagation model can be summarized as in (70)-(83).

$$V_q = V_q \cap [(P_e - V_d I_d)/I_q] \tag{70}$$

$$I_q = I_q \cap [(P_e - V_d I_d)/V_q]$$
 (71)

$$V_d = V_d \cap [(P_e - V_d I_d)/I_d] \tag{72}$$

$$I_d = I_d \cap [(P_e - V_d I_d) / V_d] \tag{73}$$

$$V_{d} = V_{d} \cap [(P_{e} - V_{d}I_{d})/I_{d}]$$
(72)

$$I_{d} = I_{d} \cap [(P_{e} - V_{d}I_{d})/V_{d}]$$
(73)

$$V_{q} = V_{q} \cap [(Q_{e} + V_{d}I_{q})/I_{d}]$$
(74)

$$I_d = I_d \cap [(Q_e + V_d I_q)/V_q]$$
 (75)

$$V_d = V_d \cap [(V_q I_d - Q_e)/I_q]$$
 (76)

$$I_q = I_q \cap \left[(V_q I_d - Q_e) / V_d \right] \tag{77}$$

$$I_d = I_d \cap \left[(E_q' - V_q) / X_d' \right] \tag{78}$$

$$E'_{d} = E'_{d} \cap [V_{d} - I_{q} X'_{q}] \tag{79}$$

$$I_q = I_q \cap [-(E_d' - V_d)/X_q']$$
 (80)

$$E'_{a} = E'_{a} \cap [V_{a} + I_{d}X'_{d}] \tag{81}$$

$$\delta = \delta \cap \left[a \sin \left(\frac{I_d}{I_{mag}} \right) + I_{ang} \right]$$
 (82)

$$\delta = \delta \cap \left[a\cos\left(\frac{I_q}{I_{mag}}\right) + I_{ang} \right]$$
 (83)

To further suppress the overestimation in the measurement equations, a simplified equation for δ is employed as (84).

$$\delta = \operatorname{atan}\left(\frac{E'_{d}}{E'_{q}}\right) + \operatorname{atan}\left(\frac{Q_{e} + X'_{d}I^{2}_{mag}}{P_{e}}\right) + I_{ang}$$
 (84)

For the state transition function h(*) in (18)-(26), the backward propagation model can be summarized as in (85)-(102).

· Synchronous generators.

$$T_M^k = T_M^k \cap \left[P'_e + D(\omega^k - \omega_s) + \frac{2H}{t_{step} * \omega_s} (\omega^{k+1} - \omega^k) \right] \tag{85}$$

$$\omega^k = \omega^k \cap \left[\frac{\omega^{k+1} - \frac{t_{step}\omega_s}{2H} (T_M - P'_e + D\omega_s)}{1 - \frac{t_{step}\omega_s D}{2H}} \right]$$
(86)

$$\delta^k = \delta^k \cap \left[\delta^{k+1} + (\omega^k - \omega_s) t_{sten} \right] \tag{87}$$

$$\omega^k = \omega^k \cap [(\delta^{k+1} - \delta^k)/t_{step} + \omega_s]$$
 (88)

$$E_q^{\prime k} = E_q^{\prime k} \cap \left[\frac{E_q^{\prime k+1} - \frac{t_{step}}{T_{d0}^{\prime}} (-(X_d - X_d^{\prime})I_d + E_{fd}^{k})}{1 - \frac{t_{step}}{T_{d0}^{\prime}}} \right]$$
(89)

$$E_{fd}^{k} = E_{fd}^{k} \cap \left[\frac{T_{d}'}{t_{step}} \left(E_{q}'^{k+1} - E_{q}'^{k} \right) + E_{q}'^{k} + (X_{d} - X_{d}') I_{d} \right]$$
(90)

$$E_d^{\prime k} = E_d^{\prime k} \cap \left[\frac{E_d^{\prime k+1} - \frac{t_{step}}{T_{q0}^{\prime}} (-(X_q - X_q^{\prime})I_q)}{1 - \frac{t_{step}}{T_{n0}^{\prime}}} \right]$$
(91)

Exciter:

$$E_{fd}^k = E_{fd}^k \cap \left[\left(E_{fd}^{k+1} - \frac{t_{step}}{T_F} V_R^k \right) / \left(1 - \frac{t_{step} K_E}{T_F} \right) \right] \tag{92}$$

$$V_{R}^{k} = V_{R}^{k} \cap \left[\frac{T_{E}}{t_{step}} \left(E_{fd}^{k+1} - E_{fd}^{k} + \frac{t_{step}K_{E}}{T_{E}} E_{fd}^{k} \right) \right]$$
(93)

$$V_F^k = V_F^k \cap \left[\frac{V_F^{k+1} - \frac{K_F t_{step}}{T_F T_E} (V_R^k - K_E E_{fd}^k)}{1 - \frac{t_{step}}{T_F}} \right]$$
(94)

$$V_R^k = V_R^k \cap \left[\frac{T_E}{K_F} \left(\frac{T_F}{t_{step}} \left(V_F^{k+1} - V_F^k \right) + V_F \right) + K_E E_{fd}^k \right]$$
(95)

$$E_{fd}^{k} = E_{fd}^{k} \cap \left[\frac{1}{K_{E}} V_{R}^{k} - \frac{T_{E}}{K_{F}K_{E}} \left(\frac{T_{F}}{t_{step}} \left(V_{F}^{k+1} - V_{F}^{k} \right) + V_{F} \right) \right]$$
(96)

$$V_{R}^{k} = V_{R}^{k} \cap \left[\left(V_{R}^{k+1} - \frac{t_{step}K_{A}}{T_{A}} \left(V_{ref} - V_{F}^{k} - V \right) \right) / (1 - \frac{t_{step}}{T_{A}}) \right] (97)$$

$$V_F^k = V_F^k \cap \left[V_{ref} - V - \frac{1}{K_A} \left(\frac{T_A}{t_{step}} \left(V_R^{k+1} - V_R^k \right) + V_R^k \right) \right] \quad (98)$$

Governor:

$$T_M^k = T_M^k \cap \left[\left(T_M^{k+1} - \frac{t_{step}}{T_{CH}} P_{SV}^k \right) / (1 - \frac{t_{step}}{T_{CH}}) \right] \tag{99}$$

$$P_{SV}^{k} = P_{SV}^{k} \cap \left[\frac{T_{CH}}{t_{step}} \left(T_{M}^{k+1} - T_{M}^{k} \right) + T_{M}^{k} \right]$$
 (100)

$$P_{SV}^{k} = P_{SV}^{k} \cap \left[\frac{P_{SV}^{k+1} - \frac{t_{Step}}{T_{SV}} \left(P_{C} - \frac{1}{R_{D}} \left(\frac{\omega^{k}}{\omega_{S}} - 1 \right) \right)}{1 - \frac{t_{Step}}{T_{SV}}} \right]$$
(101)

$$\omega^k = \omega^k \cap \left[\left(-R_D \left(\frac{T_{SV}}{t_{sten}} \left(P_{SV}^{k+1} - P_{SV}^k \right) + P_{SV}^k - P_C \right) + 1 \right) \omega_s \right] (102)$$

REFERENCES

- [1] J. Zhao et al., "Power system dynamic state estimation: motivations, definitions, methodologies, and future work," in IEEE Transactions on Power Systems, vol. 34, no. 4, pp. 3188-3198, July 2019.
- [2] Zhenyu Huang, K. Schneider and J. Nieplocha, "Feasibility studies of applying Kalman filter techniques to power system dynamic state

- estimation," 2007 International Power Engineering Conference (IPEC 2007), 2007, pp. 376-382.
- [3] S. Akhlaghi, N. Zhou and Z. Huang, "A multi-step adaptive interpolation approach to mitigating the impact of nonlinearity on dynamic state estimation," in IEEE Transactions on Smart Grid, vol. 9, no. 4, pp. 3102-3111, July 2018.
- [4] E. Ghahremani and I. Kamwa, "Dynamic state estimation in power system by applying the extended Kalman filter with unknown inputs to phasor measurements," in *IEEE Transactions on Power Systems*, vol. 26, no. 4, pp. 2556-2566, Nov. 2011.
- [5] J. Zhao, M. Netto and L. Mili, "A robust iterated extended Kalman filter for power system dynamic state estimation," in *IEEE Transactions on Power Systems*, vol. 32, no. 4, pp. 3205-3216, July 2017.
- [6] E. Ghahremani and I. Kamwa, "Online state estimation of a synchronous generator using unscented Kalman filter from phasor measurements units," in IEEE Transactions on Energy Conversion, vol. 26, no. 4, pp. 1099-1108, Dec. 2011.
- [7] N. Zhou, D. Meng and S. Lu, "Estimation of the dynamic states of synchronous machines using an extended particle filter," in IEEE Transactions on Power Systems, vol. 28, no. 4, pp. 4152-4161, Nov. 2013
- [8] Ning Zhou, Zhenyu Huang, Yulan Li and G. Welch, "Local sequential ensemble Kalman filter for simultaneously tracking states and parameters," 2012 North American Power Symposium (NAPS), pp. 1-6, 2012.
- [9] E. Ghahremani and I. Kamwa, "Dynamic state estimation in power system by applying the extended Kalman filter with unknown inputs to phasor measurements," in *IEEE Transactions on Power Systems*, vol. 26, no. 4, pp. 2556-2566, Nov. 2011.
- [10] S. Wang, J. Zhao, Z. Huang and R. Diao, "Assessing Gaussian assumption of PMU measurement error using field data," in IEEE Transactions on Power Delivery, vol. 33, no. 6, pp. 3233-3236, Dec. 2018.
- [11] F. C. Schweppe, Uncertain Dynamic Systems, Prentice-Hall, Englewood Cliffs, New Jersey: Prentice-Hall, Inc., 1973.
- [12] F. Schweppe, "Recursive state estimation: Unknown but bounded errors and system inputs," in *IEEE Transactions on Automatic Control*, vol. 13, no. 1, pp. 22-28, 1968.
- [13] E. Fogel and Y. Huang, "On the value of information in system identification—bounded noise case," in *Automatica*, vol. 18, no. 2, pp. 229-238, 1982.
- [14] F. L. Chernousko, "Ellipsoidal state estimation for dynamical systems," in *Nonlinear Analysis: Theory, Methods & Applications*, vol. 63, no. 5-7, pp. 872-879, 2005.
- [15] B. T. Polyak, S. A. Nazin, C. Durieu, and E. Walter, "Ellipsoidal parameter or state estimation under model uncertainty," in *Automatica*, vol. 40, no. 7, pp. 1171-1179, 2004.
- [16] J. S. Shamma and Kuang-Yang Tu, "Approximate set-valued observers for nonlinear systems," in *IEEE Transactions on Automatic Control*, vol. 42, no. 5, pp. 648-658, May 1997.
- [17] L. Jaulin and E. Walter, "Set inversion via interval analysis for nonlinear bounded-error estimation," in *Automatica*, vol. 29, no. 4, pp. 1053-1064, 1993.
- [18] I. Krasnochtanova, A. Rauh, M. Kletting, H. Aschemann, E. P. Hofer, and K.-M. Schoop, "Interval methods as a simulation tool for the dynamics of biological wastewater treatment processes with parameter uncertainties," in *Applied Mathematical Modelling*, vol. 34, no. 3, pp. 744-762, 2010.
 [19] L. J. Guibas, A. T. Nguyen, and L. Zhang, "Zonotopes as bounding
- [19] L. J. Guibas, A. T. Nguyen, and L. Zhang, "Zonotopes as bounding volumes," in *Proceedings of the Fourteenth Annual ACM-SIAM Symposium on Discrete Algorithms (SODA)*, vol. 3, pp. 803-812, 2003.
- [20] X. Qing, F. Yang, and X. Wang, "Extended set-membership filter for power system dynamic state estimation," in *Electric Power Systems Research*, vol. 99, pp. 56-63, 2013.
- [21] K. E. Martin et al., "IEEE standard for synchrophasors for power systems," in IEEE Transactions on Power Delivery, vol. 13, no. 1, pp. 73-77, Jan. 1998.
- [22] L. Jaulin, M. Kieffer, O. Didrit, and E. Walter, "Interval analysis," in Applied Interval Analysis, Springer, pp. 11–43, 2001.
- [23] E. Davis, "Constraint propagation with interval labels," *Artificial Intelligence*, vol. 32, no. 3, pp. 281–331, 1987.
- [24] G. Nassreddine, F. Abdallah and T. Denoux, "State estimation using interval analysis and belief-function theory: application to dynamic vehicle localization," in IEEE Transactions on Systems, Man, and Cybernetics, Part B (Cybernetics), vol. 40, no. 5, pp. 1205-1218, Oct. 2010.
- [25] T. Athay, R. Podmore and S. Virmani, "A practical method for the direct analysis of transient stability," in IEEE Transactions on Power Apparatus

- and Systems, vol. PAS-98, no. 2, pp. 573-584, March 1979.
- [26] N. Zhou, S. Wang, J. Zhao, Z. Huang, and R. Huang, "Observability and detectability analyses for dynamic state estimation of the marginally observable model of a synchronous machine," *IET Generation, Transmission & Distribution*, vol. 16, no. 7, pp. 1373-1384, 2022.
- [27] J. Zhao and L. Mili, "A decentralized H-infinity unscented Kalman filter for dynamic state estimation against uncertainties," in *IEEE Transactions* on Smart Grid, vol. 10, no. 5, pp. 4870-4880, Sept. 2019.
- [28] J. H. Chow and K. W. Cheung, "A toolbox for power system dynamics and control engineering education and research," *IEEE Transactions on Power Systems*, vol. 7, no. 4, pp. 1559-1564, 1992.
- [29] Singh, Abhinav Kumar, and Bikash C. Pal, "Report on the 68-bus, 16-machine, 5-area system," *IEEE PES Task Force on Benchmark Systems for Stability Controls*, ver. 3, 2013.
- [30] P. L. Dandeno, R. L. Hauth and R. P. Schulz, "Effects of synchronous machine modeling in large scale system studies," in *IEEE Transactions* on *Power Apparatus and Systems*, vol. PAS-92, no. 2, pp. 574-582, March 1973
- [31] I. C. Report, "Excitation system models for power system stability studies," in *IEEE Transactions on Power Apparatus and Systems*, vol. PAS-100, no. 2, pp. 494-509, Feb. 1981.
- [32] S. Akhlaghi, N. Zhou and Z. Huang, "Exploring adaptive interpolation to mitigate non-linear impact on estimating dynamic states," 2015 IEEE Power & Energy Society General Meeting, pp. 1-5, 2015.
- [33] S. Civanlar, J. Grainger, H. Yin, and S. Lee, "Distribution feeder reconfiguration for loss reduction," *IEEE Transactions on Power Delivery*, vol. 3, no. 3, pp. 1217–1223, 1988.
- [34] S.M. Rump: INTLAB INTerval LABoratory. In Tibor Csendes, editor, Developments in Reliable Computing, pages 77-104. Kluwer Academic Publishers, Dordrecht, 1999.